ISSN 0031-918X, The Physics of Metals and Metallography, 2013, Vol. 114, No. 8, pp. 692–702. © Pleiades Publishing, Ltd., 2013.
Original Russian Text © A.V. Pushin, A.A. Popov, V.G. Pushin, 2013, published in Fizika Metallov i Metallovedenie, 2013, Vol. 114, No. 8, pp. 753–764.

STRUCTURE, PHASE TRANSFORMATIONS, AND DIFFUSION

Effect of Deviations of Composition from the Quasi-Binary Section TiNi–TiCu on Structural and Phase Transformations in Rapidly Quenched Alloys

A. V. Pushin[a, b], A. A. Popov[b], and V. G. Pushin[a, b]

[a] *Institute of Metal Physics, Ural Branch, Russian Academy of Sciences, ul. S. Kovalevskoi 18, Ekaterinburg, 620990 Russia*

[b] *The First President of Russia B. N. Yeltsin Ural Federal University (UrFU), ul. Mira 28, Ekaterinburg, 620002 Russia*

e-mail: avpushin@rambler.ru, pushin@imp.uran.ru

Received August 24, 2012; in final form, November 28, 2012

Abstract—Methods of X-ray diffraction, transmission and scanning electron microscopy, and selected-area electron diffraction (SAED) have been used to study the phase and elemental composition and structure of alloys close to the stoichiometric $Ti_{50}Ni_{25}Cu_{25}$ alloy. Based on the method of rapid quenching of the melt (free-jet melt spinning), alloys of the quasi-binary TiNi–TiCu section have been prepared, which in the initial as-cast state exhibited the thermoelastic martensitic transformations $B2 \leftrightarrow B19$ and related shape-memory effects. The chemical composition of the $Ti_{50+x}Ni_{25}Cu_{25-x}$ alloys was varied by changing titanium and copper concentrations within $x \le \pm 1$ at % (from $Ti_{49}Ni_{25}Cu_{26}$ to $Ti_{51}Ni_{25}Cu_{24}$). It has been established that quenching at a cooling rate equal to 10^6 K/s leads to the amorphization of all the alloys under consideration. Heating to 723 K and higher leads to the devitrification of the alloy with the formation of a nanocrystalline or submicrocrystalline structure of the $B2$ austenite. The mechanical properties of these alloys have been measured in the initial amorphous state and in the polycrystalline martensitic state. It has been shown that, depending on the extent of the deviations of the alloy composition from the stoichiometry, which cause the decomposition of the alloys in the process of nanocrystallization, regular changes are observed in their mechanical properties and in the shape-memory effects. The kinetics of the processes of the devitrification of the alloys, as well of the forward and reverse martensitic transformations, have been studied, their characteristic temperatures have been determined, and a diagram of the dependence of the characteristic temperatures on the chemical composition of the alloys has been constructed.

Keywords: Ti_2NiCu-based alloys ($Ti_{50}Ni_{25}Cu_{25}$), rapid quenching of alloys by free-jet melt spinning, nanocrystals, thermoelastic martensitic transformations, shape-memory effects

DOI: 10.1134/S0031918X13060136

INTRODUCTION

One of practically important discoveries of the 20th century was the discovery of thermoelastic martensitic transformations (TMTs) and related shape-memory effects (SMEs), which are inherent in a novel class of functional and, simultaneously, structural materials [1, 2]. In this group of materials, the alloys based on titanium nickelide have the best complex of practically important characteristics: very high strength and plastic properties; uniquely high effects of thermomechanical memory; high reliability; high mechanothermal, mechanocyclic, and thermocyclic durability, weldability, corrosion resistance; biological compatibility, etc. [2–6]. These alloys have a relatively simple chemical composition and exhibit good technological efficiency from the viewpoint of metallurgical and subsequent production processing [2–6].

Nevertheless, the application of these alloys in the conventional polycrystalline as-cast state or after many well-known heat or thermomechanical treatments by no means always ensures high physicomechanical characteristics of articles required in practice. The necessity of obtaining substantially higher strength properties of the alloys in the form of small-dimension semiproducts with the retention or even improvement of a complex of functional parameters of the SME has initiated one of the approaches, primarily in the cases of ternary Ti–Ni–Cu alloys, that is based on the use of methods of ultrarapid quenching from the melt (RQM), in particular, the method of free-jet melt spinning, to produce very long, very thin ribbons with an SME [7–22].

In our previous work [23], we have studied the main specific features of the structure, phase and elemental composition, and properties of nonstoichiometric

$Ti_{50-x}Ni_{25+x}Cu_{25}$ alloys ($x \le \pm 1$ at %) for the first time. To obtain these SME alloys in a high-strength nanocrystalline state in the form of thin ribbons, here, we again employed the method of free-jet melt spinning. It has been shown that the RQM at a cooling rate of 10^6 K/s produces the amorphization of all these alloys. Heating to 723 K and higher temperatures leads to the devitrification of these alloys via polymorphous, primary, or eutectic mechanisms without a change or with a change in the chemical composition upon the formation of the polycrystalline structure of the *B*2 austenite, according to Hornbogen [24]. It has turned out that the polycrystalline $Ti_{50-x}Ni_{25+x}Cu_{25}$ alloys are homogeneous solid solutions or undergo phase separation and become precipitation-hardening solutions depending on the extent of nonstoichiometry. On the contrary, in the $Ti_{50}Ni_{25}Cu_{25}$ alloy of stoichiometric composition, the crystallization and subsequent recrystallization occur without changes in the chemical composition. It has been revealed that, depending on the extent of the deviations of the alloy composition from stoichiometry in terms of titanium and nickel, which lead to the nanocrystallization and phase separation in these alloys, the mechanical properties and SMEs of the ribbons change in a regular manner. In this case, the ultimate strength σ_u and the yield stress $\sigma_{0.2}$ of the ribbons vary in a wide range, but the plasticity remains good, and the high values of the reactive stress are retained (difference between the yield stress $\sigma_{0.2}$ and the phase martensitic pseudo-yield stress σ_m), as well as of the satisfactory reversible deformation. The values of the critical temperatures of the start and finish of the devitrification of the alloys and of the forward and reverse TMTs in them have been determined.

In this work, we performed a complex investigation of nonstoichiometric RQM alloys $Ti_{50+x}Ni_{25}Cu_{25-x}$ with a composition that was varied in terms of titanium and copper within x of up to ± 1 at %.

EXPERIMENTAL

The ribbons of the alloys were prepared by the method of free-jet melt spinning at a cooling rate $v_q = 10^5$ and 10^6 K/s. For the investigations, ten RQM alloys of the Ti–Ni–Cu system have been selected, whose chemical composition deviated from the $Ti_{50+x}Ni_{25}Cu_{25-x}$ stoichiometry by changing titanium and copper concentrations in steps of ± 0.25 at %. The samples, the thickness of which was varied from 25 to 60 μm by changing the regime of the setup for the rapid quenching from the melt, were studied both in the initial (as-quenched) state and after nanocrystallization by annealing at 723 and 773 K for 10 min.

The electron-microscopic investigations were performed at the Electron Microscopy Center of Collaborative Access, Institute of Metal Physics, Ural Branch, Russian Academy of Sciences, using a scanning electron microscope (Quanta 200, FEI Company, the Netherlands) and transmission electron microscopes (Tecnai G^2-30 Twin, FEI Company, the Netherlands; and JEM-200 CX, JEOL, Japan). For phase identification, the method of selected-area electron diffraction (SAED) using standard selector diaphragms was employed. The chemical composition was controlled by the method of energy-dispersive X-ray analysis using EDAX spectrometers with which the microscopes of the FEI Company are equipped. The X-ray diffraction investigations were performed by the $\theta/2\theta$ method in the reflection mode using a DRON-3M diffractometer in Cu $K\alpha$ radiation monochromatized by a graphite single crystal. The X-ray diffraction investigations were performed upon heating in situ using a standard GPVT-2000 high-temperature vacuum attachment. The electrical resistivity was measured in situ in the temperature range of 100–770 K on samples shaped as rectilinear ribbons 40 mm long. The rates of heating and cooling of the samples were 2.5 K/min. The mechanical strength and plastic characteristics were measured using tensile tests at room temperature in an Instron tensile machine. The microhardness was determined using a PMT-3M device with a diamond indentation pyramid. To estimate the deformation characteristics of the SME in the produced RQM alloys, the effect of bending deformation on the degree of shape recovery upon heating was studied.

RESULTS AND DISCUSSION

The X-ray diffraction and electron-microscopic investigations have shown that all the samples of the $Ti_{50+x}Ni_{25}Cu_{25-x}$ alloys after RQM at a rate $v_q = 10^6$ K/s (in contrast to quenching at a rate of 10^5 K/s) at room temperature are in amorphous state. Figure 1 presents fragments of typical X-ray diffraction patterns of the alloys studied. The X-ray diffraction patterns of amorphous alloys contain, near the expected positions of the Bragg reflections of the *B*2 austenite or *B*19 martensite, only diffuse and very wide maxima. The widest and most intense ($\Delta 2\theta$ reaches 10–12 deg, Fig. 1, curve *1*) diffuse maximum is located near the position of the first fundamental line 110_{B2}. In electron micrographs and SAED patterns, a typical salt–pepper contrast and diffuse halos are observed, respectively (Fig. 2). In the dark-field images taken using the diffuse halo, highly dispersed regions a few nanometers in size are shining (Fig. 2b). The X-ray diffraction peaks against the background of diffuse maxima have been revealed only after annealing of the amorphous alloys at 673–693 K (Fig. 1, curve *2*); after annealing at 773 K, they completely replace the diffuse maxima and have been identified as reflections of the *B*2 austenite or *B*19 martensite (Fig. 1, curves *3* and *4*, respectively).

The kinetics of the processes of the devitrification and subsequent TMT in the alloys, just as the characteristic temperatures of the start (T_s) and finish (T_f) of crystallization upon heating from the amorphous state

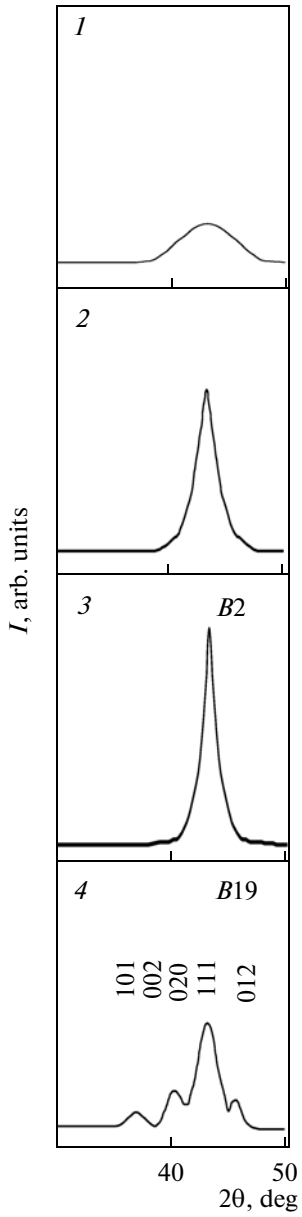

Fig. 1. Fragments of X-ray diffraction patterns of RQM quasi-binary TiNi–TiCu alloys (quenching rate $v_q = 10^6$ K/s) taken (*1*) in the initial state and in the experiments in situ in the regimes of heating to (*2*) 693 and (*3*) 773 K and subsequent cooling (*4*) to room temperature.

(obtained by RQM at a rate $v_q = 10^6$ K/s) and the critical temperatures of the start and finish of the forward and reverse TMTs were determined mainly from the temperature dependences of the electrical resistivity $\rho(T)$ measured at a rate of heating equal to approximately 2 K/min. A typical example of this dependence is shown in Fig. 3.

It follows from Fig. 3 that the isochronous annealing of an amorphous alloy at below ~570 K does not change the behavior of the $\rho(T)$ curve in the heating–cooling cycle, which indicates the absence of structural changes in the alloy. Further heating, however, leads to a sharp drop in the electrical resistivity in the range of 700–720 K. In the course of subsequent cooling from 770 K, the decrease in the resistivity first continues; then, an increase occurs, followed by a decrease in ρ with the formation of narrow hysteresis upon the reverse heating, which indicates the presence of the $B2 \leftrightarrow B19$ TMT with the critical temperatures of the start and finish of the forward and reverse TMTs determined to be $M_s = 330$ K, $M_f = 300$ K, $A_s = 308$ K, $A_f = 338$ K.

Upon the further analysis of the results of investigations, the isothermal annealing at 723 K for 10 min was chosen as the main (the same for all the alloys) treatment. Based on the results of [23], it was assumed that this treatment would reveal the effect of the chemical composition (deviations from the stoichiometric composition) on the process of the devitrification and its main structural and morphological characteristics. As a consequence, the revealed regularities and, first of all, the structural mechanism of the crystallization of amorphous RQM ribbons would make it possible to explain the behavior of the physicomechanical properties and to develop principles of controlling the SME of the alloys under investigation.

The electron-microscopic and electron-diffraction investigations of the RQM alloys subjected to a heat treatment at 723 K for 10 min have shown the following. The alloy of a stoichiometric composition $Ti_{50}Ni_{25}Cu_{25}$ at room temperature in the state of *B*19 martensite has a typical packet–pyramidal morphology of lamellar pairwise-twinned crystals (Fig. 4). The orientation relationships (ORs) between the *B*19 martensite and *B*2 austenite are close to Bain ORs [23]

$$\begin{aligned} [100]_{B19} &\parallel \langle 100 \rangle_{B2}; \\ [010]_{B19} &\parallel \langle 0\bar{1}1 \rangle_{B2}; \\ [001]_{B19} &\parallel \langle 011 \rangle_{B2}. \end{aligned} \quad (1)$$

Analysis has shown that the average size of the initial *B*2 austenite grains that arise as a result of the above heat treatment is 1.0–1.5 μm. A noticeable decrease in the dimensions of grains of the *B*2 austenite is caused by deviations from stoichiometry in titanium and copper at a fixed content of nickel (25 at %). At deviations by ±0.25, ±0.50, and ±0.75 at %, the average size of grains of the *B*2 austenite decreases to approximately 800–900, 500–600, and 250–300 nm, respectively (Figs. 5, 6). The *B*19 martensite partly retains its twinned substructure. In the alloys with the deviations in titanium and copper by 1 at %, the size of grains of the *B*2 austenite decreased to 20–30 nm (i.e., by a factor of 30–50 as compared to the alloy of stoichiometric composition $Ti_{50}Ni_{25}Cu_{25}$). Thus, the average size of nanocrystallites in the alloys with an excess or deficit of titanium by 1 at % is close to 30 nm (Figs. 7, 8). Nevertheless, all these alloys at room temperature

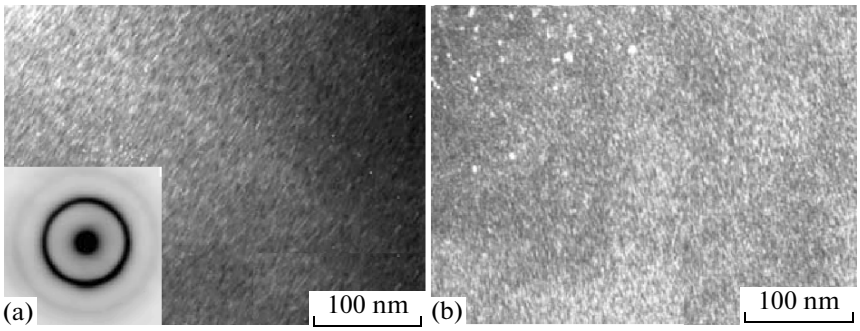

Fig. 2. (a) Bright-field and (b) dark-field electron micrographs and corresponding SAED pattern (in the inset in (a)) of the $Ti_{50.5}Ni_{25}Cu_{24.5}$ alloy in the as-quenched condition (after RQM at a rate $v_q = 10^6$ K/s).

were (mainly, judging from the SAED patterns and $\rho(T)$ data) in the state of the *B*19 martensite.

Thus, the annealing of amorphous alloys with a composition deviated by ±1 at % Ti or Cu from the stoichiometric composition at 723 K for 10 min leads to their nanocrystallization (Figs. 7 and 8). In this case, the positions of reflections in the SAED patterns proved to be fundamentally different; their ringlike arrangement indicates that the nanocrystallites have an arbitrary distribution with respect to crystallographic orientations. It has been revealed that the martensite in the nanostructured alloys contains no planar defects (nanotwins or stacking faults). As was shown by the investigations performed, the microstructure of the alloys is characterized by a highly homogeneous distribution of the arising nanocrystals. As for the features of the diffraction contrast in the micrographs in the form of two arcs or rings (Figs. 7, 8), we note that, following the theory of contrast, their origin appears to be related to the fields of elastic stresses near the boundaries of nanograins of the *B*19 martensite.

Passing now to a quantitative analysis of electron diffraction patterns, note that the RQM alloys studied appear to refer in their chemical composition to the class of decomposing solid solutions based on the atomically ordered *B*2-type compound $Ti_{50}Ni_{25}Cu_{25}$ in which one of the sublattices is occupied by titanium atoms and in the other sublattice the nickel and copper atoms are distributed in a random way. According to neutron-diffraction data, the degree of long-range atomic order η in this alloy is equal to 0.90 ± 0.05 [22]. No diagrams of phase equilibria in these ternary alloys have been revealed in the literature, except for the TiNi–TiCu quasi-binary section.

In accordance with [24], it would be reasonable to suppose that, in the process of low-temperature heat treatments, and even more so upon devitrification, in the second phases of the studied nonstoichiometric alloys excess two-component phases can be formed, such as Ti_3Ni_4, Ti_2Ni, and TiCu, depending on the supersaturation of the $Ti_{50}Ni_{25}Cu_{25}$ solid solution by alloying elements. These phases are formed in the case when excessive concentrations of concrete chemical elements relative to the basic composition $Ti_{50}Ni_{25}Cu_{25}$ exist in the alloy. These elements have been revealed in the course of the identification of a number of SAED patterns. It has turned out that many reflections are nearly coincident, although there are also reflections that are noncoincident from the viewpoint of interplanar spacings, which makes it possible to unambiguously identify them. Thus, in alloys with a titanium concentration of 51 at %, two nanophases of the Ti_2Ni and TiCu type have been revealed (Fig. 7, Table 1) and, in alloys with a titanium content of 49 at %, two nanophases of the Ti_3Ni_4 and TiCu type have been found (Fig. 8). It was difficult to identify their precipitation based on dark-field images, since it is impossible to even separate their own closely spaced reflections. However, in the bimodal distribution of nanocrystallites, the finer particles are apparently the precipitates of excessive phases. Table 1 contains the electron-diffraction constant *K* of the instrument, the distance to the corresponding reflection *r*, the experimentally calculated values of the interplanar spacings d_p, the tabulated values of the interplanar spacings d_t calculated using corresponding quadratic formulas, and the

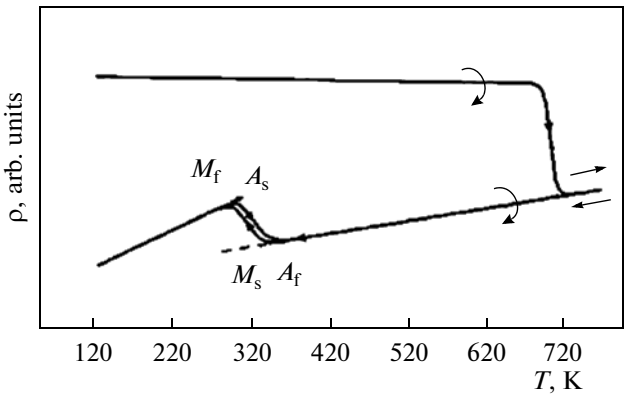

Fig. 3. Temperature dependence of the electrical resistivity $\rho(T)$ of the amorphous $Ti_{50}Ni_{25}Cu_{25}$ alloy quenched from the melt at a rate $v_q = 10^6$ K/s and subjected to heating to 773 K, cooling to 123 K, and heating to 373 K.

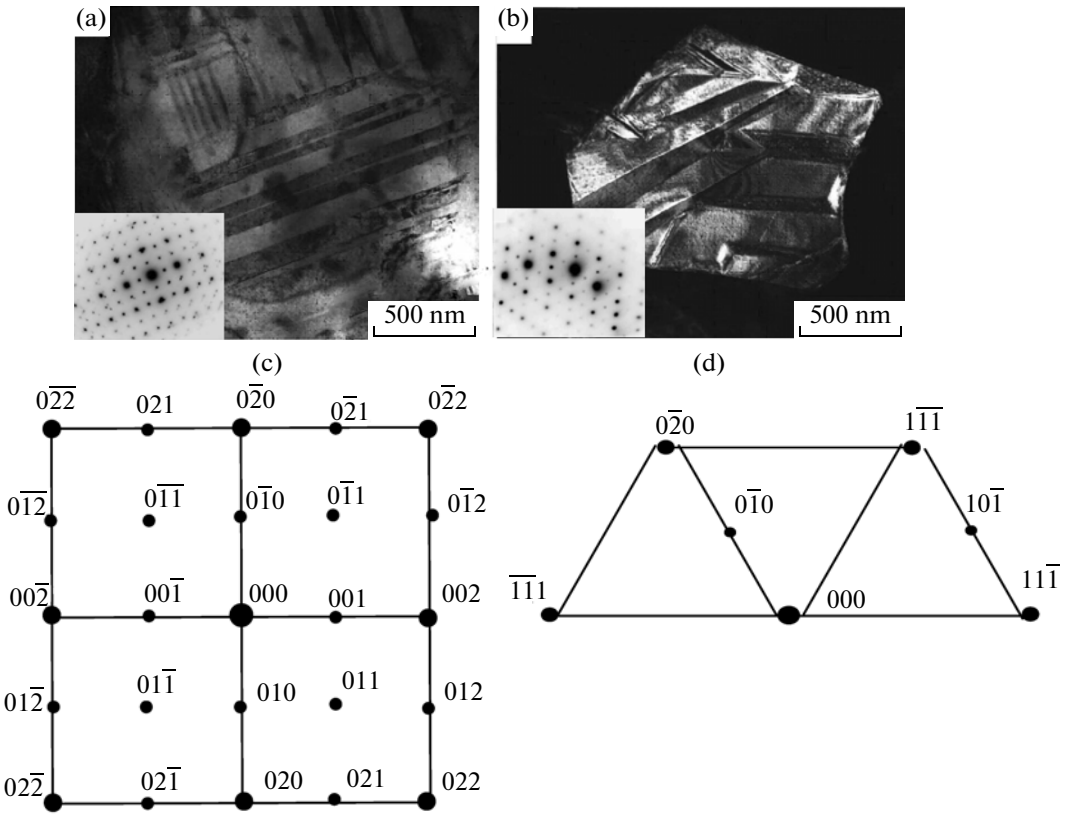

Fig. 4. (a) Bright-field and (b) dark-field electron micrographs and the corresponding SAED patterns (in the insets: reciprocal-lattice sections (a) $(100)_{B19}$ and (b) $(101)_{B19}$) of the $Ti_{50}Ni_{25}Cu_{25}$ alloy after annealing at (a) 773 K and (b) 723 K for 10 min; (b) a dark-field micrograph taken in reflection $0\,\bar{1}0_{B19}$; and (c, d) the key patterns to the SAED patterns given in the insets in (a) and (b), respectively.

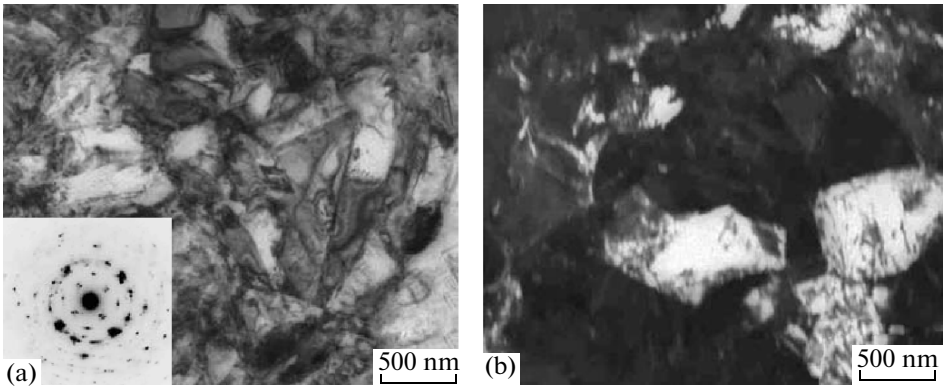

Fig. 5. (a) Bright-field and (b) dark-field electron micrographs and the corresponding SAED pattern (in the inset in (a)) of the $Ti_{50.50}Ni_{25}Cu_{24.50}$ alloy produced by RQM at a rate $v_q = 10^6$ K/s and subjected to annealing at 723 K for 10 min.

corresponding interference indices *HKL* of the matrix *B*19 martensite and second phases Ti_2Ni and TiCu.

To refine the interpretation of the obtained data on the phase composition of the alloys (and, first of all, of the second phases), an amorphous alloy with greater deviations from the stoichiometry in both titanium and copper ($Ti_{52}Ni_{25}Cu_{23}$) has been prepared by the RQM method (using a quenching rate $v_q = 10^6$ K/s). Figure 9 presents bright-field and dark-field images of the nanostructure and the corresponding SAED patterns of this alloy after annealing at 723 K for 10 min. The calculations of the electron diffraction patterns showed that, after such heat treatment in the nanocrystalline alloy $Ti_{52}Ni_{25}Cu_{23}$, two phases should be

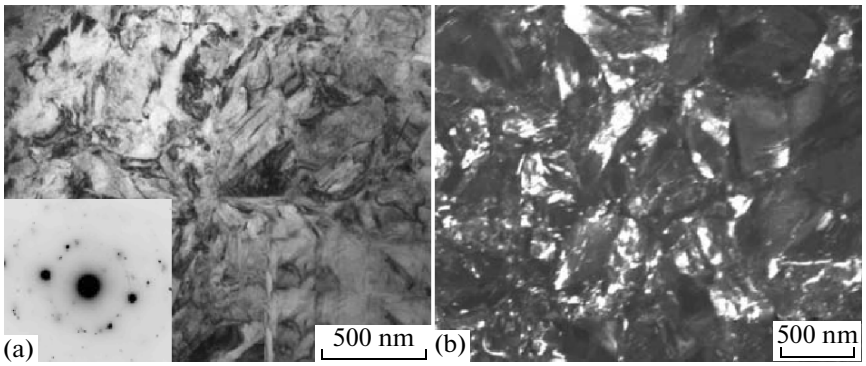

Fig. 6. (a) Bright-field and (b) dark-field electron micrographs and the corresponding SAED pattern (in the inset in (a)) of the $Ti_{49.25}Ni_{25}Cu_{24.75}$ alloy produced by RQM at a rate $v_q = 10^6$ K/s and subjected to annealing at 723 K for 10 min.

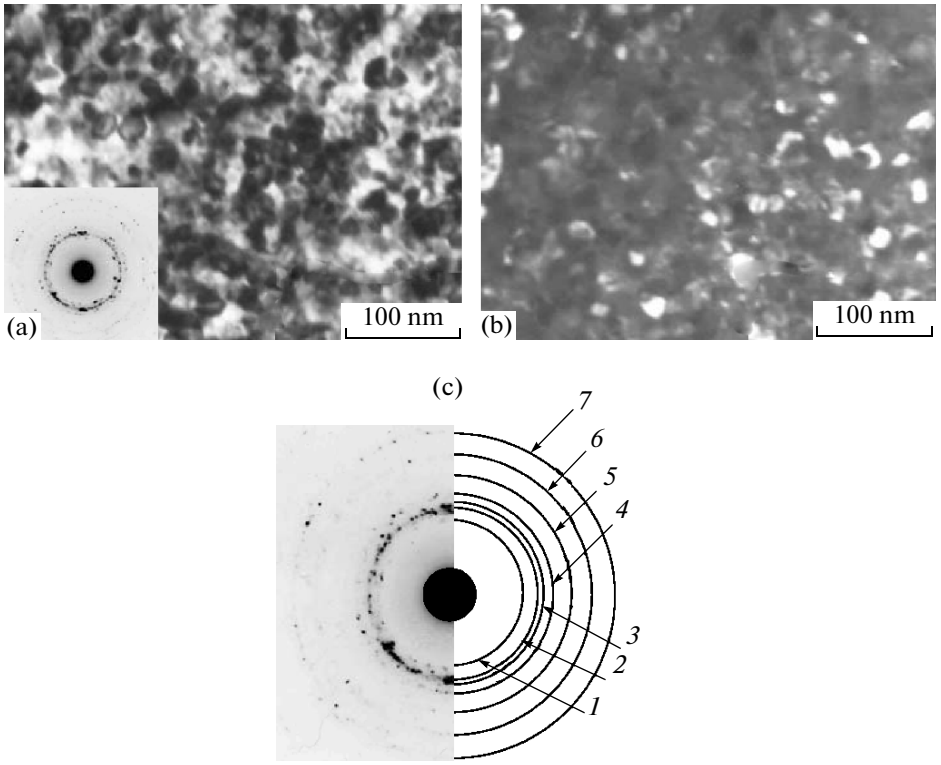

Fig. 7. (a) Bright-field and (b) dark-field electron micrographs and the corresponding SAED patterns (in the inset in (a) and in Fig. 7c (with a related key pattern)) of the $Ti_{51}Ni_{25}Cu_{24}$ alloy produced by RQM at a rate $v_q = 10^6$ K/s and subjected to annealing at 723 K for 10 min.

present at room temperature, i.e., the matrix martensite ($B19$) and a second phase Ti_2Ni. Thus, this experiment additionally confirms the formation of second phases in nonstoichiometric alloys upon their nanocrystallization from the amorphous state.

Based on the concepts developed by Hornbogen [24], it can be assumed that, in the amorphous alloy $Ti_{50}Ni_{25}Cu_{25}$, upon heat treatment, polymorphous or massive directional crystallization occurs, in which the chemical compositions of both phases, i.e., both the amorphous phase and crystalline $B2$ phase, remain almost unaltered. In the alloys that differ only insignificantly from the stoichiometric composition in terms of titanium and copper under the same conditions of heat treatment, the crystallization is accompanied by the refinement of the grain structure to submicron dimensions, i.e., their grain size decreases twofold or threefold compared to the stoichiometric alloy; however, no second phases have been revealed and, at room temperature, only $B19$ martensite was identified. It is obvious that the slowing-down of the rate of crystal growth up to their mutual joining is mainly

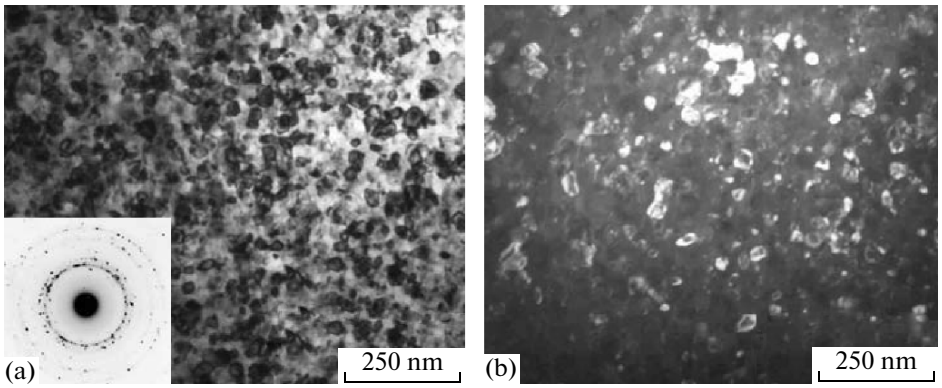

Fig. 8. (a) Bright-field and (b) dark-field electron micrographs and the corresponding SAED pattern (in the inset in (a)) of the $Ti_{49}Ni_{25}Cu_{26}$ alloy produced by RQM at a rate $v_q = 10^6$ K/s and subjected to annealing at 723 K for 10 min.

caused by the effect of the concentration gradients of those chemical elements in which the alloy is weakly supersaturated relative to $Ti_{50}Ni_{25}Cu_{25}$; their supersaturation is partly eliminated inside *B*2 crystallites, whereas, around these crystallites, the concentration of these elements is excessive. Therefore, unlike the case of massive crystallization, the development of this mechanism, which is called "primary crystallization" and occurs with a change in the chemical composition [23, 24], is slowed down somewhat and, since the number of nuclei will increase upon heat treatment, in the final account, the crystallization is completed by an increase in the dispersity of the grain structure. The continuation of heat treatment after the exhaustion of both polymorphous and primary crystallization can lead to the subsequent preferentially heterogeneous decomposition.

In the alloys that are supersaturated to a greater extent with respect to the $Ti_{50}Ni_{25}Cu_{25}$ alloy (as was found, upon a deviations from stoichiometry by ±1 at % or greater), the mechanism of crystallization is accompanied by phase decomposition with the formation of excessive phases, e.g., via a eutectic reaction [23, 24]. In this case, the devitrification occurs without any intermediate via a complex mechanism with the formation of a highly disperse metastable globular nanoduplex (two-phase), nanotriplex (three-phase), or nanocomplex (multiphase) morphology of the mixture of a Ti(Ni,Cu) phase (*B*2' type) and TiCu, Ti_2Ni, and Ti_3Ni_4 phases. Generally speaking, in the case of all of the above-described mechanisms of crystalliza-

Table 1. Identification of ringlike electron diffraction pattern of $Ti_{51}Ni_{25}Cu_{24}$ alloy

No.	K, mm Å	r, mm	d_p, Å	d_t, Å	HKL_{B19}	d_t, Å	HKL_{TiCu}	d_t, Å	HKL_{Ti_2Ni}
1	22.5	8.2	2.7	–	–	2.74	101	–	–
2	22.5	10.0	2.3	2.26	002	2.19	110	2.30	422
3	22.5	10.5	2.1	2.14 2.13	020 111	2.13	102	2.17	511
4	22.5	11.4	2.0	2.00	012	2.05 1.96	111 003	1.99	440
5	22.5	13.6	1.7	1.73 1.65	120 112	1.66	103	1.63 1.58	444 551
6	22.5	16	1.4	1.46 1.42 1.39 1.36 1.34	200 013 201 031 103	1.46 1.39 1.37 1.35	113 210 202 211	1.41 1.38	800 733
7	22.5	18.5	1.2	1.23 1.23 1.23 1.21 1.21	023 202 131 220 032	1.25 1.22	212 203	1.24 1.23 1.18	911 842 931

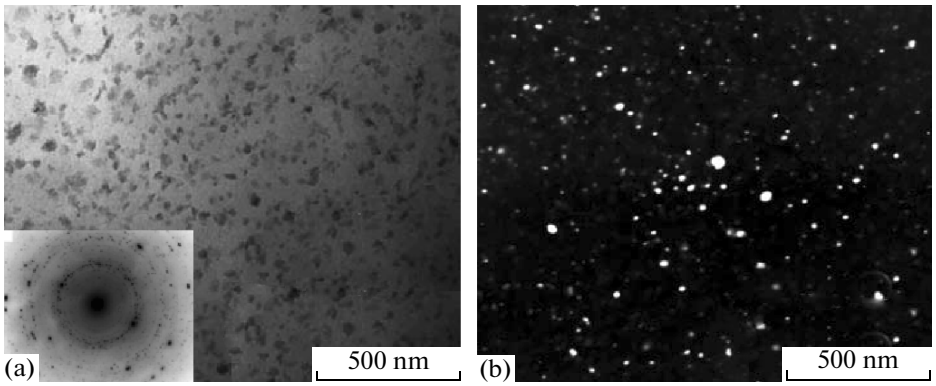

Fig. 9. (a) Bright-field and (b) dark-field electron micrographs taken using a group of reflections 002_{B19}, 020_{B19}, 111_{B19}, 110_{B11}, 102_{B11}, and 511_{Ti_2Ni} closely spaced in the rings, and the corresponding SAED pattern (in the inset in (a)) of the $Ti_{52}Ni_{25}Cu_{23}$ alloy produced by RQM at a rate $v_q = 10^6$ K/s and subjected to annealing at 723 K for 10 min.

tion, after its completion, the structural state in the *B*2 alloys under consideration remains nonequilibrium with respect to both the chemical and the phase composition, as well as to the dimensional and morphological characteristics. Therefore, during the subsequent heat treatment, secondary processes of recrystallization of the matrix *B*2 phase, as well as of the evolution of both excessive phases and mechanisms of decomposition, e.g., via a changeover from the heterogeneous mechanism of their nucleation to a homogeneous mechanism, will unavoidably develop.

The dimensions and the chemical composition of grains of the *B*2 matrix, as well as the types and dimensions of excessive phases in the TiNi-based alloys determine the specific features of the TMTs and related physicomechanical properties and SMEs, including their force, deformational, and temperature parameters. Here, it is important to note that the revealed dependences of the martensitic points, mechanical properties and SMEs on the chemical nonstoichiometry of the $Ti_{50}Ni_{25}Cu_{25}$-type alloys have a more complex nature caused by the nanosize effect due to the refinement of the grain structure in the process of crystallization, which is in turn determined by the barrier chemical or phase effect.

The tensile tests of the mechanical properties of RQM alloys at room temperature have shown the following. Under tension, the amorphous alloys undergo brittle fracture; the stage of strain hardening is nearly absent in them, but the elastic deformation at fracture reaches $\delta_{el} = 4\%$ in them. As a rule, the stress–strain diagrams are linear. The ultimate tensile strength of the alloys of stoichiometric composition is equal to 1200 MPa and increases up to 1800 MPa with the deviation from the stoichiometry by ±1 at %. The same RQM alloys after additional annealing at 723 K for 10 min have a different grain structure and phase composition. Depending on the chemical composition (and degree of nonstoichiometry), the deformation-related yield stress $\sigma_{0.2}$ changes from 680 to 1200 MPa, the ultimate tensile strength σ_u changes from 850 to 1550 MPa, and the reactive stress σ_r changes from 620 to 1110 MPa (Fig. 10, Table 2). The relative elongation δ is retained within 10–12%, and the length of the plateau of the phase pseudoyield, which is caused by the

Table 2. Mechanical properties of RQM alloys

Alloy	Heat treatment		σ_m, MPa	$\sigma_{0.2*}$, MPa	σ_u, MPa	σ_r, MPa	ε_{pel}, %	δ, %
	Quenching rate, K/s	Temperature of the isothermal annealing for 10 min						
$Ti_{51}Ni_{25}Cu_{24}$	10^6	773	90	1200	1550	1110	3.0	12.0
$Ti_{49}Ni_{25}Cu_{26}$	10^6	773	90	1150	1380	1060	3.0	12.0
$Ti_{50.75}Ni_{25}Cu_{24.25}$	10^6	723	80	1100	1280	1020	3.5	11.0
$Ti_{50.50}Ni_{25}Cu_{24.50}$	10^6	773	80	1050	1170	970	3.5	9.5
$Ti_{49.50}Ni_{25}Cu_{25.50}$	10^6	773	80	950	1120	870	3.5	10.0
$Ti_{49.75}Ni_{25}Cu_{25.25}$	10^6	773	50	750	900	700	4.0	10.0
$Ti_{50}Ni_{25}Cu_{25}$	10^5	773	60	680	850	620	5.0	10.0

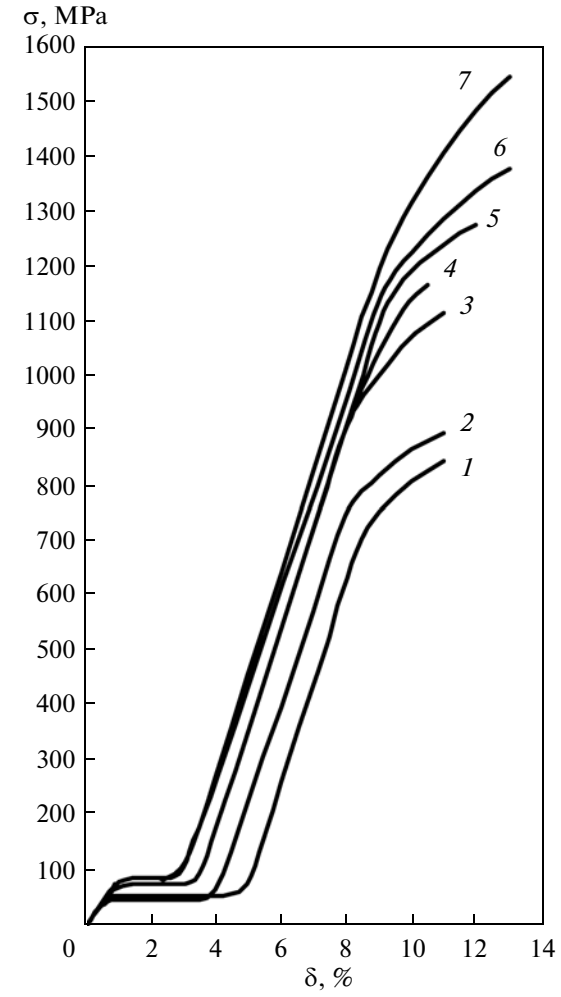

Fig. 10. Tensile stress–strain diagrams of ribbons of polycrystalline alloys (*1*) $Ti_{50}Ni_{25}Cu_{25}$, (*2*) $Ti_{49.75}Ni_{25}Cu_{25.25}$, (*3*) $Ti_{49.50}Ni_{25}Cu_{25.50}$, (*4*) $Ti_{50.5}Ni_{25}Cu_{24.5}$, (*5*) $Ti_{50.75}Ni_{25}Cu_{24.25}$, (*6*) $Ti_{49}Ni_{25}Cu_{26}$, and (*7*) $Ti_{51}Ni_{25}Cu_{24}$ produced by RQM at a rate $v_q = 10^6$ K/s and subjected to heat treatment at 723 K for 10 min.

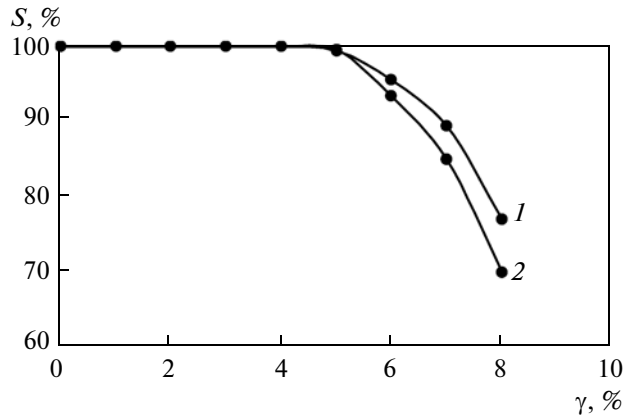

Fig. 11. Dependence of (*1*, *2*) the degree of restoration *S* of the SME of the RQM alloys $Ti_{50}Ni_{25}Cu_{25}$ on the degree of deformation by bending γ at room temperature after annealing for 10 min at (*1*) 723 and (*2*) 773 K.

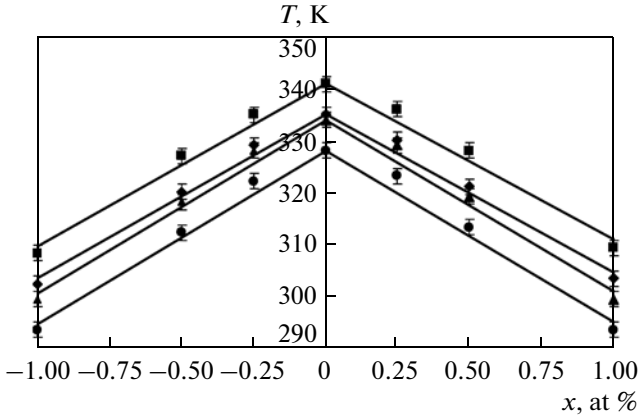

Fig. 12. Critical temperatures of the start and finish of the forward and reverse TMTs as functions of chemical composition of $Ti_{50-x}Ni_{25}Cu_{25+x}$ alloys produced by RQM at a quenching rate $v_q = 10^6$ K/s and subjected to annealing at 723 K for 10 min: (■) A_f, (◆) M_s, (▲) A_s, and (●) M_f.

pseudo-elastic deformation of martensite ε_{pel}, somewhat changes (from 3 to 5%).

The limit of phase martensitic pseudoyield σ_m also increases, though to a lesser extent (from 60 to 90 MPa), remaining less than $\sigma_{0.2}$ by an order of magnitude. Since the temperatures of the start of the forward TMT, M_s, and, as a rule, of the finish of the TMT, M_f, of these alloys are close to or exceed room temperature, the alloys are already in the martensitic state. Their anelastic deformation at a stress equal to the limit of the martensitic pseudo-elastic deformation σ_m is implemented at the pseudo-yield plateau, mainly via the pseudo-elastic reorientation of martensitic crystals in the direction of the acting force [1–5].

The microhardness of amorphous alloys has high values (7000–7500 MPa), whereas the microhardness of the crystalline alloys of the same composition is significantly less (3000–5000 MPa). The deformation characteristics of the SME of the alloys are shown in Fig. 11. It can be seen that the complete restoration of the shape ($S = 100\%$) of the sample that has been bent at room temperature occurs after deformation γ up to 4–5%. After greater degrees of deformation (γ = 6–7%), the magnitude of *S* decreases to 80–70%. A further increase in deformation (to γ = 8%) leads to the brittle fracture of the ribbon upon bending.

The temperature dependences of the electrical resistivity ρ(*T*) measured in this work have been systemized in the form of a diagram of the TMTs (dependences of the critical temperatures of the start and finish of the forward and reverse TMTs on the magnitude of *x*, which characterizes the degree of nonstoichiometry of the chemical composition of the alloys) shown in Fig. 12. It has been established that the deviations of the chemical composition of the alloys of the quasi-binary section TiNi–TiCu from stoichiometry in tita-

Table 3. Dependence of the critical temperatures of the TMT on the chemical composition of the RQM $Ti_{50-x}Ni_{25}Cu_{25+x}$ alloys (quenching rate $v_q = 10^6$ K/s) subjected to annealing at 723 K for 10 min (the error of measuring temperature is ±1 K)

x	A_f, K	M_s, K	A_s, K	M_f, K
−1.00	308	302	299	293
−0.50	327	320	318	312
−0.25	335	329	328	322
0.00	341	335	334	328
0.25	336	330	329	323
0.50	328	321	319	313
1.00	309	303	299	293

nium and copper leads to changes in the critical temperatures. Both with increasing titanium concentration (to 51 at %) and decreasing copper content (to 24 at %) and, on the contrary, with decreasing titanium concentration (to 49 at %) and increasing copper concentration (to 26 at %), the critical temperatures of the TMTs decrease significantly (Table 3).

CONCLUSIONS

Thus, after heat treatment, the alloys with SME based on the stoichiometric composition $Ti_{50}Ni_{25}Cu_{25}$ in the form of long, thin, high-strength ribbons produced by the method of free-jet melt spinning possess fairly high strength properties, transformation-induced plasticity (reversible deformation), and relative elongation. The variation in their chemical composition due to changing concentrations of titanium and copper (within ±1 at %) makes it possible to precisely control the critical temperatures of the start and finish of the forward and reverse thermoelastic martensitic transformation (TMTs) in practically important ranges of 29–62°C, 20–55°C, 26–61°C, and 35–68°C, respectively. The results of the identification of X-ray diffraction patterns and the data on the chemical composition obtained by energy-dispersive X-ray analysis have not revealed the presence of possible excessive (second) phases in the alloys after their devitrification under the chosen regimes of heat treatment. An analysis of the selected-area electron-diffraction (SAED) patterns with a ringlike distribution of reflections made it possible to identify excess reflections (additional in comparison to those from the $B2$ and $B19$ phases), which, according to calculations, correspond to phases of the Ti_2Ni, Ti_3Ni_4, and TiCu types and are excessive with respect to the stoichiometric alloy.

By comparing the data on the chemical composition of the RQM alloys, their microstructure (and, first of all, the average size of $B2$ grains), phase composition, critical temperatures of the TMTs, and mechanical properties, it may be concluded that the following four main factors are responsible for the observed effects:

(1) the effect of deviations proper of the chemical composition of the initial alloys from that of the stoichiometric Ti_2NiCu alloy;

(2) the existence of processes of crystallization and phase decomposition in $B2$ solid solutions supersaturated with respect to the stoichiometric Ti_2NiCu composition in the course of heat treatments;

(3) the grain refinement upon the crystallization of amorphous alloys due to the barrier action of nonstoichiometric alloying or due to already precipitated disperse second phases;

(4) the development of highly reversible $B2 \leftrightarrow B19$ TMTs and the size effect of the $B2$ grains on their critical temperatures.

ACKNOWLEDGMENTS

This work was supported in part by the Presidium of the Russian Academy of Sciences (grant no. 12-P-2-1060, 12-2-005-Arktika) and by the Russian Foundation for Basic Research (project no. 11-02-00021).

REFERENCES

1. G. V. Kurdjumov and L. G. Khandros, "On the thermoelastic equilibrium at martensitic transformations," Dokl. Akad. Nauk SSSR **66**, 211–214 (1949).
2. K. Otsuka, K. Shimizu, Y. Suzuki, Y. Sekiguchi, C. Tadaki, T. Honma, and S. Miyazaki, *Shape Memory Alloys*, Ed. by H. Funakubo (Kyoto, 1984; Metallurgiya, Moscow, 1990).
3. V. N. Khachin, V. G. Pushin, and V. V. Kondrat'ev, *Titanium Nickelide: Structure and Properties* (Nauka, Moscow, 1992) [in Russian].
4. V. G. Pushin, V. V. Kondrat'ev, and V. N. Khachin, *Pretransition Phenomena and Martensite Transformations* (Ural. Otd. Ross. Akad. Nauk, Ekaterinburg, 1998) [in Russian].
5. V. G. Pushin, S. D. Prokoshkin, R. Z. Valiev, V. Brailovskii, E. Z. Valiev, A. E. Volkov, A. M. Glezer, S. V. Dobatrin, E. F. Dudarev, V. T. Zhu, Yu. G. Zainulin, Yu. R. Kolobov, V.V. Kondratiev, A. V. Korolev, A. I. Korshunov, N. I. Kourov, N. V. Kudrevatykh, A. I. Lotkov, L. L. Meisner, A. A. Popov, N. N. Popov, A. I. Razov, M. A. Khusainov, Yu. I. Chumlyakov, S. V. Andreev, A. A. Baturin, S. P. Belyaev, V. N. Grishkov, D. V. Gunderov, A. P. Dyupin, K. V. Ivanov, V. I. Itin, M. K. Kasymov, O. A. Kashin, I. V. Kireeva, A. I. Kozlov, T. E. Kuntsevich, N. N. Kuranova, N. Yu. Pushina, E. P. Ryklina, A. N. Uksusnikov, I. Yu. Khmelevskaya, A. V. Shelyakov, V. Ya. Shklover, E. V. Shorokhov, and L. I. Yurchenko, *Titanium Nickelide Alloys with Shape Memory. Ch. I. Structure, Phase Transformations and Properties* (Ural. Otd. Ross. Akad. Nauk, Ekaterinburg, 2006) [in Russian].
6. V. G. Pushin, "Alloys with a termomechanical memory: structure, properties and application," Phys. Met. Metallogr. **90** (Suppl. 1), S68–S95 (2000).

7. S. P. Alisova, N. V. Lutskaya, P. V. Budberg, and E. I. Bychkova, "Phase structure of TiCu–TiNi–TiCo (TiFe) systems in equilibrium and metastable states," Izv. Ross. Akad. Nauk., Ser. Met., No. 3, 221–228 (1993).
8. M. B. Babanly, V. A. Lobodyuk, and N. M. Matveeva, "Characteristics and structural peculiarities of martensite quenched from the melt," Izv. Ross. Akad. Nauk., Ser. Met., No. 5, 171–177 (1993).
9. N. M. Matveeva, V. G. Pushin, A. V. Shelyakov, Yu. A. Bykovskii, S. B. Volkova, and V. S. Kraposhin, "Effect of the conditions of crystallization of amorphous TiNi–TiCu alloys on their structure and shape memory," Phys. Met. Metallogr. **83**, 623–632 (1997).
10. V. G. Pushin, S. B. Volkova, and N. M. Matveeva, "Structural and phase transformations in quasi-binary TiNi–TiCu alloys rapidly quenched from the melt: I. High-copper amorphous alloys," Phys. Met. Metallogr. **83**, 275–282 (1997).
11. V. G. Pushin, S. B. Volkova, and N. M. Matveeva, "Structural and phase transformations in quasi-binary TiNi–TiCu alloys rapidly quenched from the melt: II. Alloys with mixed amorphous–crystalline structure," Phys. Met. Metallogr. **83**, 283–288 (1997).
12. V. G. Pushin, S. B. Volkova, and N. M. Matveeva, "Structural and phase transformations in quasi-binary TiNi–TiCu alloys rapidly quenched from the melt: III. Mechanisms of crystallization," Phys. Met. Metallogr. **83**, 435–443 (1997).
13. V. G. Pushin, S. B. Volkova, and N. M. Matveeva, "Structural and phase transformations in quasi-binary TiNi–TiCu alloys rapidly quenched from the melt: IV. The microstructure of crystalline alloys," Phys. Met. Metallogr. **83**, 673–678 (1997).
14. V. G. Pushin, S. B. Volkova, N. M. Matveeva, L. I. Yurchenko, and A. S. Chistyakov, "Structural and phase transformations in quasi-binary TiNi–TiCu alloys rapidly quenched from the melt: V. Effect of heat treatment," Phys. Met. Metallogr. **83**, 679–683 (1997).
15. V. G. Pushin, S. B. Volkova, N. M. Matveeva, L. I. Yurchenko, and A. S. Chistyakov, "Structural and phase transformations in quasi-binary TiNi–TiCu alloys rapidly quenched from melt: VI. Martensitic Transformations," Phys. Met. Metallogr. **84**, 441–448 (1997).
16. V. G. Pushin, N. I. Kourov, T. E. Kuntsevich, N. N. Kuranova, N. M. Matveeva, and L. I. Yurchenko, "Nanocrystalline TiNi-based shape-memory materials produced by ultrarapid quenching from melt," Phys. Met. Metallogr. **94** (Suppl. 1), S107–S118 (2002).
17. V. G. Pushin, V. V. Popov, T. E. Kuntsevich, N. I. Kourov, and A. V. Korolev "Rapidly quenched TiNiCo alloys with shape-memory effect: I. Martensitic transformations and mechanical properties," Phys. Met. Metallogr. **91**, 374–382 (2001).
18. V. G. Pushin, V. V. Popov, T. E. Kuntsevich, and N. M. Matveeva, "Rapidly solidified shape-memory TiNiCo alloys: II. Microstructure," Phys. Met. Metallogr. **91**, 486–493 (2001).
19. V. G. Pushin, N. I. Kourov, T. E. Kuntsevich, N. M. Matveeva, and V. V. Popov, "Structure and properties of rapidly quenched TiNiFe alloys with a shape memory effect: I. Microstructure and phase composition of initial austenite," Phys. Met. Metallogr. **92**, 58–62 (2001).
20. V. G. Pushin, N. I. Kourov, T. E. Kuntsevich, N. M. Matveeva, and V. V. Popov, "Structure and properties of rapidly quenched TiNiFe alloys with a shape memory effect: II. Martensite transformations and properties," Phys. Met. Metallogr. **92**, 63–69 (2001).
21. V. A. Aleksashin, V. V. Kondrat'ev, A. V. Korolev, A. V. Pushin, V. G. Pushin, A. V. Soloninin, and A. P. Tankeev, "^{63}Cu NMR spectra, magnetic susceptibility, and transmission electron microscopy of the rapidly quenched alloy $Ti_{50}Ni_{25}Cu_{25}$," Phys. Met. Metallogr. **110**, 582–587 (2010).
22. V. G. Pushin, N. N. Kuranova, A. V. Pushin, E. Z. Valiev, N. I. Kourov, A. E. Teplykh, and A. N. Uksusnikov, "Formation of nanocrystalline structure in the amorphous $Ti_{50}Ni_{25}Cu_{25}$ alloy upon severe thermomechanical treatment and the size effect of the thermoelastic martensitic $B2 \leftrightarrow B19$ transformation," Phys. Met. Metallogr. **113**, 271–282 (2012).
23. A. V. Pushin, A. A. Popov, and V. G. Pushin, "Effect of the deviation of the chemical composition from the stoichiometric composition on the structural and phase transformations and properties of rapidly quenched $Ti_{50+x}Ni_{25-x}Cu_{25}$ alloys," Phys. Met. Metallogr. **113**, 283–294 (2012).
24. E. Khornbogen, "Phase structure and microstructure of rapidly quenched alloys," in *Fourth International Conderence on Rapidly Quenched Metals*, Ed. by S. Steeb and W. Warlimont, Wurzburg, 1984 (Elsevier, Amsterdam, 1985), pp. 785–796.

Translated by S. Gorin